Current Science
CS 6 (5), 6595-6609 (2026)
Received 23 July 2026 | **Accepted 15 August** 2026 | **Online Available 03 September** 2026
https://doi.org/10.52845/CS/2026-6-5-1

Current Science

Current Science

OPEN ACCESS

ISSN (O) 2795-8639

Original Article

Utilization of Silkworm Pupae-Derived Biochar for Cr (VI) Removal

Qin-wen Zheng[1], Qin-jin Wei[2], Zhi-peng Zhang[3], Shan-shan Guo[2], Jin-yan Yang[2], Xiao-ke Guo[4], and Yuan-yue Liu[4,*]

[1]**Sichuan Province Environmental Monitoring Station, Chengdu 610074, China**

[2]**College of Architecture and Environment, Sichuan University, Chengdu 610065, China**

[3]**Sichuan Geological Environment Survey and Research Center, Chengdu 610081, China**

[4]**Sichuan Academy of Eco-Environmental Sciences, Chengdu 610041, China**

These two affiliations (1 and 4) are considered co-first contributing institutions

***Corresponding Author: Yuan-yue Liu**

Abstract:
Silkworm pupae, a prevalent agricultural residue in China, are rich in proteins and polysaccharides, offering significant potential for resourceful utilization. This study investigates the application of silkworm pupa-derived biochar for the removal of hexavalent chromium [Cr(VI)] from water. Biochar was produced through pyrolysis at 300 °C, 400 °C, and 500 °C at varying retention times. The silkworm pupa biochar produced at 300 °C exhibited effective Cr(VI) removal under acidic conditions (pH < 3), at a relatively low temperature of 15 °C, and with an adsorbent dosage below 5 g/L, reaching a maximum adsorption capacity of 1.476 mg/g. The adsorption process was consistent with the pseudo-second-order kinetic equation and the Freundlich isotherm adsorption model, which indicate that the adsorption of Cr(VI) by the biochar proceeded simultaneously with membrane diffusion and intraparticle diffusion. Some oxygen-containing functional groups and C=C groups were involved in the adsorption process. The study highlights the feasibility of using silkworm pupa biochar as a sustainable and economically viable adsorbent for wastewater remediation. These findings provide a potential approach for utilizing agricultural waste in environmental management, contributing to both waste treatment and pollution control.
Keywords: adsorption, biochar, economic feasibility, heavy metal, water

Introduction

With an annual cocoon production of about 751,700 tons in China, silkworm pupae have become a prevalent agricultural by-product (Chinese National Statistics Bureau, 2024). Currently, silkworm pupae are primarily processed for use as feed and fertilizer (Altomare *et al.* 2020). In addition, due to the high protein and polysaccharide (chitin and chitosan) content of silkworm pupae, they can be used to prepare biochar (Febrianto *et al.* 2009). With its advantages in high surface area, micro-porosity, ion exchange capacity and abundance in feedstock (Ahmad *et al.* 2014), biochar has been used in soil remediation, carbon sequestration, solid waste combustion, and wastewater treatment (Beesley *et al.* 2010; Ahmad *et al.* 2014). Researchers have taken interest in many organic wastes no matter plant or animal derived biomass. Grass (Wilson *et al.* 2025), wood (Keiluweit *et al.* 2010), straw (Chen *et al.* 2011), animal manure (Kołodyńska *et al.* 2012) and sewage sludge (Wiedner *et al.* 2013) are common raw materials to generate biochar. Biochar derived from plant sources has dominated previous research, while the application of silkworm pupae-derived biochar in water remediation remains largely

unexplored. Biochar derived from different materials exhibit different crystalline properties under different preparation conditions (Keiluweit *et al.* 2010), which affect their physicochemical properties (pH, ash content, polarity, surface structure, surface functional groups, etc.) (Cantrell *et al.* 2012). This leads to different environmental behavior and affects their applications.

Chromium (Cr) is one of the heavy metals that have different oxidation states, which mainly presents in the oxidation states of trivalent chromium [Cr(III)] and hexavalent chromium [Cr(VI)] in environment (Kotaś & Stasicka 2000). Cr(VI) is highly cumulative and significantly more toxic than Cr(III) (Kotaś & Stasicka 2000). Long-term exposure to Cr(VI) can cause kidney and liver damage, as well as damage to the circulatory system and nerve tissues (Giri *et al.* 2012). The Cr concentration in rivers and lakes is usually limited to 0.5~100 nM, and in sea waters it varies from 0.1 ~16 nM (Kotaś & Stasicka 2000). However, the Cr concentration in industrial effluents from electronics, electroplating, metallurgical, leather tanning and wood preservatives exceeds the standards far beyond (Altundogan 2005).

This study aims to explore the potential of silkworm pupa-derived biochar (SPB) as an adsorbent for remediating Cr(VI)-contaminated water. The influence of key preparation parameters, specifically pyrolysis temperature and retention time, on biochar yield and Cr(VI) removal efficiency was investigated under controlled conditions. The objective is informing the rational design of biochar-based adsorbents for heavy metal contaminated water remediation.

2 Materials and Methods

2.1 Biomass Pyrolysis for Biochar Production

Dry silkworm pupa was purchased from an agriculture store (Er ni all's store for green and healthy food) in China. The silkworm pupa was ground to a particle size of less than 0.77 mm, and transferred into lidded ceramic crucibles. Pyrolysis was subsequently carried out in a muffle furnace under an oxygen-limited atmosphere at a heating rate of approximately 15 °C min^{-1} (Onay & Kockar 2003). The pyrolysis temperatures were set at 300 ℃, 400 ℃, and 500 ℃, respectively, and maintained for durations varying among 0.5 h and 2 h, followed by cooling to room temperature. After grinding to a particle size of less than 0.15 mm, the SPB biochar was stored in airtight containers. The resulting products are designated as BC300/time, BC400/time, and BC500/time, respectively, to reflect the corresponding pyrolysis temperature and holding time.

The pH of the biochar was determined in a 1:20 (w/v) suspension, prepared by mixing 0.5 g of sieved sample (0.15 mm) with 10 mL of CO_2-free deioned water (Wang *et al.* 2018). All measurements were performed in triplicate. The surface morphology of the biochar was characterized by using a field emission scanning electron microscope (SEM) (JSM-7500F, JEOL, Japan) (Mao *et al.* 2023). Functional groups of BC400/2 before and after adsorption were analyzed by Fourier transform infrared spectroscopy (FTIR) (Nicolet 6700, Thermo Fisher Scientific, USA).

2.2 Adsorption and Desorption Experiments

The effects of adsorption time, temperature, solution pH, the additive dose of SPB, and the coexisting ion on Cr remove were estimated. The pH of Cr containing solution ranged from 2.0 to 9.0 was adjusted by using 1% hydrochloric acid and 1 M sodium hydroxide. The 10 mg/L original Cr(VI) solution with 0.5 g adsorbent was employed to conduct adsorption kinetic experiments. The dosage experiments were carried out by adding 0.05, 0.1, 0.2, 0.5 and 1.0 g adsorbent in 50 mL polythene centrifuge tubes containing 10 mL Cr(VI) solution (10 mg/L) at the ratio (w:v) of 5, 10, 20, 50 and 100 g/L,

respectively, under the optimum pH. Absorption experiments were conducted at 15 ℃, 25 ℃, and 35 ℃, respectively, to imitate different solution temperature. The SPB was equilibrated with Cr(VI) solutions on a horizontal shaker at 200 rpm for designed time under optimal temperature. Desorption was conducted after the adsorption reaction under the optimum circumstances in 1 M sodium hydroxide solution (Shi *et al.* 2018). The Cr(VI) concentration was attained using an UV-vis spectrophotometer (U-4100, Dongguan Hongcheng Optical Products Co., LTD, China) (Shi *et al.* 2018). The concentration of total Cr in the solution after adsorption under optimal temperature was analyzed by an ICP-MS (NEXION 300X, PE, America). The concentration of Cr(III) was calculated as the difference between the total Cr and Cr(VI) concentrations (Mao *et al.* 2023). Three replicates of each sample were performed. The adsorption capacity (q_e) was calculated as follows *(Jia et al.* 2021):

$$q_e = \frac{(C_0 - C_e)\cdot V}{m} \qquad (1)$$

where q_e is the adsorption capacity of Cr(VI) as the equilibrium achieved, mg/g; C_0 is the initial Cr(VI) concentration in solution before adsorption, mg/L; C_e is the equilibrium concentration after adsorption, mg/L; V represents the volume of initial Cr(VI) solution, L; and m is for the mass of adsorbents, g (Luo *et al.* 2022).

2.3 Kinetics and Isotherm Adsorption Studies

Pseudo-first order kinetic model, pseudo-second order kinetic model, and intra-particle diffusion model were used to analyse the Cr(VI) adsorption kinetics (Ma *et al.* 2021). Two isotherm models (Langmuir and Freundlich models) were chosen to describe the adsorption isotherm data (He *et al.* 2019; Ma *et al.* 2021). These equations are displayed in Table 1.

Table 1. Kinetic and isotherm models used in this study

	Types	Equations
Kinetics models	Pseudo-first-order	$q_t = q_e\left(1 - exp(-k_1 t)\right)$
	Pseudo-second-order	$\frac{t}{q_t} = \frac{1}{k_2 {q_e}^2} + \frac{1}{q_e} t$
	Intra-particle diffusion	$q_t = k_d t^{0.5} + C$
Isotherm models	Langmuir	$q_e = \frac{k_L q_m C_e}{1 + k_L C_e}$
	Freundlich	$q_e = K_F \cdot {C_e}^{1/n}$

where, t is the adsorption time, min; k_1 is the first-order rate constant, min^{-1}; k_2 is the second-order rate constant, g/(mg·min); q_e is the adsorption capacity, mg/g; q_t is the adsorption capacity in time t, mg/g; k_d is the rate constant of intra-particle diffusion, g/mg; C is the intercept; q_m is the maximum adsorption capacity, mg/g; C_e is the equilibrium concentration of adsorbate, mg/L; k_L is adsorption equilibrium constant, L/mg; n is the surface heterogeneity factor, representing the adsorption strength; and K_F is adsorption capacity (Ma *et al.* 2021) .

2.4 Statistical Analysis

All batch isotherms were run in triplicate with blank runs and averaged with standard deviation. All laboratory appliance used in the study was previously soaked in HNO_3 solution for at least 12 h, rinsed three times with distilled water and oven-dried before use. Regression analysis of experimental data was performed using Sigma Plot V9.0 for Windows statistical software (SPSS

Inc.). One-way and two-way ANOVA were used to test the significance between the experimental and control groups.

3 Results and Discussion

3.1 Biochar Yield

Compared to most of plant derived biochars which were prepared under temperatures higher than 500 ℃ and underwent long retention time (2~8 h) (Wang & Wang 2019), the preparation of the SPB in the present study was under lower temperature and in shorter time. The highest biochar yield was approximately 72.9% at a pyrolysis temperature of 300 °C and a retention time of 1 h. Biochar yields of the silkworm pupa decreased significantly (p<0.05) as pyrolysis temperature increased from 300 ℃ to 400 ℃ and 500 ℃ (Table 2), where most of the thermal decomposition of protein materials occurs (Suliman *et al.* 2016). At the same time, the yield had a significant decrease as retention time prolonged within a higher temperature range. These phenomena suggest that at relatively low temperatures (300 ℃), increasing the retention time has less effect on the reduction of char yield than at higher temperatures (400 ℃ and 500 ℃). These phenomena indicated that at 300 ℃ to 500 ℃, shortening retention time can significantly improve SPB yield. Similar phenomenon was also observed during the preparation of plant-derived biochar (Braadbaart & Poole 2008).

Table 2. Biochar yield under different pyrolysis temperature and retention time

Pyrolysis temperature/°C	Heating speed/(°C/min)	Retension time/h	Biochar yield
300	10~15	1	72.9%±1.0%^{a}
		2	68.7%±11.5%^{ab}
400	10~15	0.5	50.6%±0.3%^{bc}
		1	28.1%±1.4%^{cde}
		2	26.9%±3.7%^{d}
500	10~15	1	20.2%±1.5%^{d}
		2	14.7%±0.9%^{e}

* a, b, c, d, and e stand for significant difference in one-way ANOVA using Tamhane's testing at p<0.05.

The nonlinear relationship between pyrolysis temperature along with retention time and the pH of the biochar is shown in Fig. 1a. The results of two-way ANOVA analysis taking pyrolysis temperature and retention time as dominate factors showed that retention time did not have a significant effect on the pH of the biochar. In a relative low temperature range (300~400 °C in this case), the pH of the biochar increased with pyrolysis temperature increasing. However, the increase of pH didn't follow this tendency under higher temperature range (400 °C and 500 °C), which was also found in a previous study discussing the influence of pyrolysis temperature and retention time on pH of biochar, which was produced by corn cob, soybean stalk and rice husk (Zhang *et al.* 2013). The loss of bio-acid as well as the enrichment of mineral elements led to the increase of pH under different pyrolysis temperature and retention time (Novak *et al.* 2009). The increased retention time didn't have a clear impact on the pH of the biochar compared to the influence of pyrolysis temperature. As the residence time increasing, the formation of high boiling point materials (Uchimiya *et al.* 2011) and the slow oxidization of inherent recalcitrant aromatic ring structure (Nguyen *et al.* 2009) occur at the same time, leading to a complex impact on the pH of the biochar.

Increasing the pyrolysis temperature as well as lengthening retention time had a significant impact on the removal ability of Cr(VI) by the biochars (Fig. 1b). The adsorption performance of the BC300/4 was better than that of the rest of the biochars, indicating that SPB had a better Cr(VI) removal ability prepared under a relatively low temperature range (300~400 °C in this case) due to the higher specific surface area (Uchimiya *et al.* 2011) and the larger amount of active functional groups (Du *et al.* 2008). Lengthening the residence time had a negative effect on Cr(VI) removal in this case, despite the fact that inadequate retention time would leading to the incomplete oxidation of the inherent recalcitrant aromatic ring structure, thus influencing the hydrophilicity of biochar.

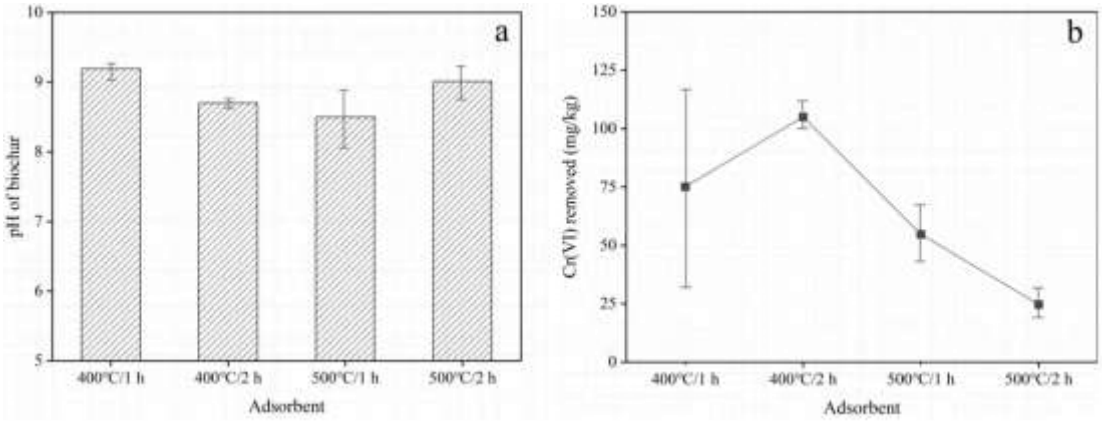

Fig. 1. pH and Cr(VI) removal ability of biochar prepared under different temperature and retention time. (a) pH; (b) Cr(VI) removal ability. Lowercase letters a and b in the figures stand for significant difference in two-way ANOVA using LSD according to pyrolysis temperature; capital letters A and B in the figures stand for significant difference in two-way ANOVA using LSD according to retention time.

3.2. Main Factors Effect on the Removal of Cr(VI)

Although the Cr(VI) removal capacity by BC300/4 was high, the pyrolysis temperature needed to be held for 4 h, which consumed more time and energy. At pyrolysis temperature of 500°C, the biochar yield and Cr(VI) removal capacity was low. Therefore, BC400/2 was selected for adsorption experiments considering energy loss, pyrolysis time, biochar yield and Cr(VI) removal capacity.

3.2.1. Effect of Adsorption Temperature on Cr(VI) Removal

The adsorption behavior of Cr(VI) on the SPB was different from that of previous Cr adsorption experiment where the removal rate increased with adsorption temperature (Giri *et al.* 2012). In the present study, the Cr(VI) removal rate by BC400/2 was 58.6%, 38.5%, and 46.2% at 15 °C , 25 °C, and 35 °C, respectively (Fig. 2a). This may be due to the change of surface porosity and active adsorption site of the biochar with the increase of temperature. Cr(VI) reduction took 25% of total Cr(VI) removal at 2 hours of adsorption reaction (Fig. 2b), which was close to the proportion of Cr adsorbed on sugar beet tailing derived biochar (Dong *et al.* 2011). Less than 12% of adsorbed Cr(VI) was desorbed at 15°C (Fig. 2a), suggesting that the majority of the reaction was irreversible (Davis *et al.* 2003).

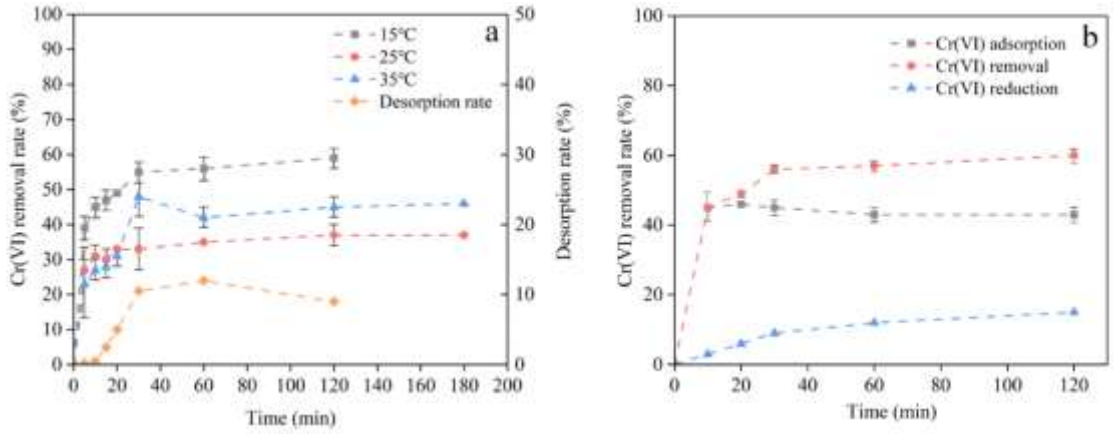

Fig. 2. Effect of temperature on removal rate of Cr(VI) by BC400/2 and desorption of adsorbed Cr(VI). (a) Initial Cr(VI) concentration = 10 mg/L, BC400/2 = 5 g/L (w : v), and pH = 2.85; (b) The proportion of Cr(VI) adsorption, desorption and reduction under 15 °C, initial Cr(VI) concentration = 10 mg/L, BC400/2 = 5 g/L (w : v), and pH = 2.85

3.2.2 Effect of pH on Cr(VI) Removal

A significant decrease in removal efficiency was observed as the solution pH increased from 2.85 to 3.05 (Fig. 3a). The highest removal efficiency achieved at pH 2.85, which was consistent with previous work where the best removal rate of Cr(VI) was found under the pH range from 1~3 (Maryuk *et al.* 2005). At Cr(VI) concentrations up to 10^{-2} M, $HCrO_4^-$ is the predominant form at solution pH 6.5 (Kotaś & Stasicka 2000), and $HCrO_4^-$ is believed easier to interact with adsorbents compared to other forms of Cr(VI) (Álvarez-Ayuso *et al.* 2007). In addition, some researchers proposed that amino groups of chitosan could be protonated under pH 4, where electrostatic interaction occurs between the adsorbent and $HCrO_4^-$ ions, resulting in high Cr(VI) removal from the water (Aydın & Aksoy 2009).

3.2.3. Effect of Biochar Dosage on Cr (VI) Removal

The removal efficiency of Cr(VI) decreased by adding more SPB into the solution at additive range from 10 g/L to 100 g/L (Fig. 3b). In the study by Giri *et al.* (2012), activated carbon prepared from Eichhornia crassipes root biomass was employed as an adsorbent. The removal rate of Cr(VI) increased with the adsorbent dosage rising from 1 g/L to 7 g/L, beyond which no significant further enhancement was observed. The reduction of removal rate in the present study can be attributed to the overlap of available surface areas of the adsorbant, which causes particle agglomeration and thereby decreases Cr(VI) adsorption capacity at higher adsorbent dosages (Dakiky *et al.* 2002).

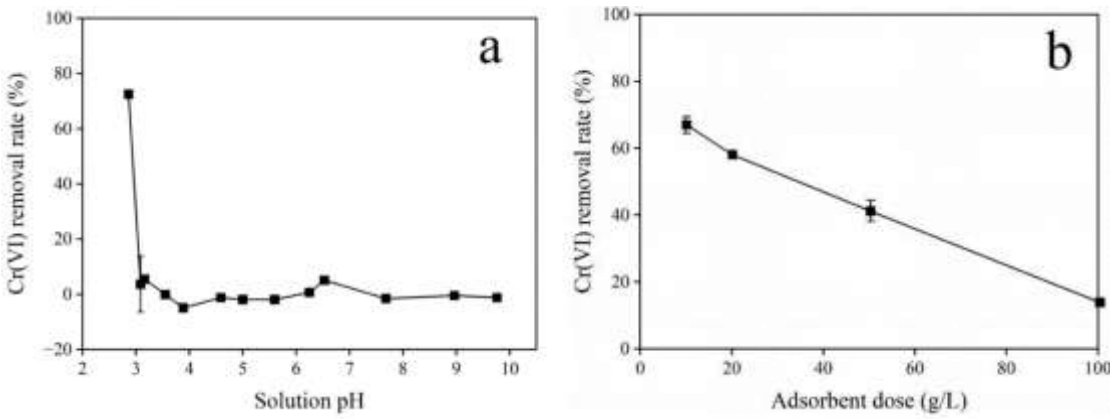

Fig. 3. The effect of solution pH (a) and additive dose (b) on Cr(VI) removal. Initial Cr(VI) concentration = 10 mg/L, BC400/2 = 5 g/L (w : v), and T = 15 °C

3.3. Adsorption Kinetics and Thermodynamics

The BC400/2 exhibited near-maximum adsorption capacity for Cr(VI) within 2 hours in a Cr(VI) concentration range of 5–100 mg/L, with the adsorption capacity being notably enhanced at elevated temperatures. The exact equilibrium adsorption quantity is hard to estimate because much longer equilibrium period follows the initial rapid adsorption (McKay *et al.* 1999). Pseudo-first-order model (Fig. 4a) as well as the pseudo-second-order model (Fig. 4b) well described the reaction between the biochar and Cr(VI) in the solution (Gupta & Bhattacharyya 2011). Higher R^2 of the pseudo-second-order model was found than that of the pseudo-first-order model, indicating that there was more than a single layer adsorption between the biochar and Cr(VI). Experimental maximum adsorption capacity (1.476 mg/g) was close to the theoretical maximum adsorption capacity in theory based on the pseudo-second-model (1.516 mg/g), which lay within the typical adsorption capacity of 0.7~22 mg/g (Natale *et al.* 2007). Pseudo-second-order model is classic to calculate the theoretical maximum adsorption capacity but it was highly temperature dependent and hard to make proper predictions (McKay *et al.* 1999). Judging from R^2 of both the kinetic models, the pseudo-second-order model were more precise to describe the adsorption of Cr(VI) by BC400/2, which means the chelation site played a critical role in the adsorption. In addition, there was an apparent turning point in the relationship between q_t and $t^{1/2}$ taking apart the adsorption procedure into two processes in intra-particle diffusion model (Fig. 4c). The first portion was the gradual adsorption stage where the intra-particle diffusion can be rate controlling (Noroozi *et al.* 2007). The second portion is the final equilibrium stage where the intra-particle diffusion started to slow down (Febrianto *et al.* 2009). Time spent for particle transition shortened from 30 min to 20 min when temperature increased from 15 °C to 35 °C (Fig. 4c). The q_t versus $t^{1/2}$ plot did not go through the origin, indicating that both film diffusion and intraparticle diffusion occured simultaneously during the process of Cr(VI) adsorption by BC400/2 (Ozcan *et al.* 2006).

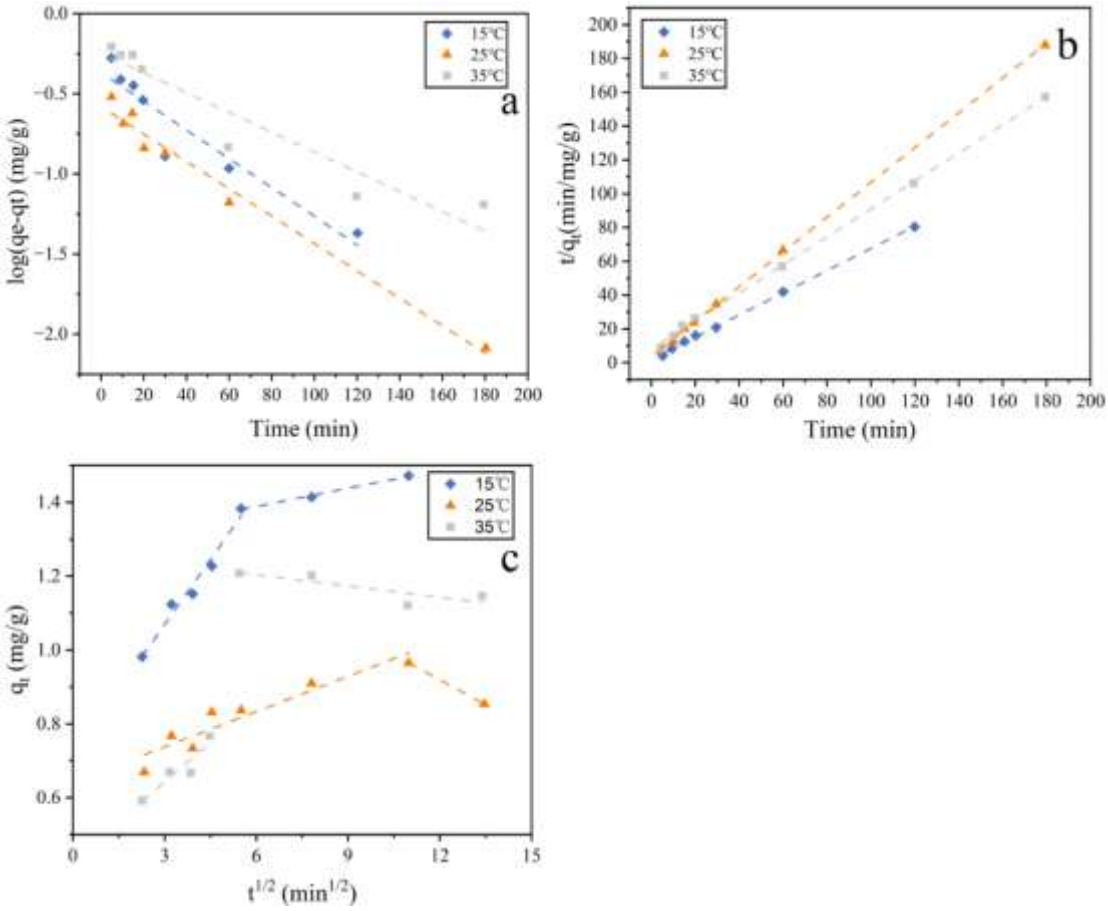

Fig. 4. Pseudo-first-order model, Pseudo-second-order model and Intra-particle model of Cr(VI) removal by BC400/2. (a) Pseudo-first-order model; (b) Pseudo-second-order model; (c) Intra-particle model.

Langmuir and Freundlich models are commonly used to draw adsorption isotherms (Ma *et al.* 2021). The Langmuir model can properly describe the uniform adsorption (Febrianto *et al.* 2009). The value of K_L indicates the type of isotherm to be unfavorable (K_L > 1), linear (K_L = 1), irreversible (K_L = 0) or favorable (0 < R_L <1) (Weber & Chakravorti 1974). When K_L is close to 0, it means the reaction is irreversible and one of the premise of Langmuir model is broken (Weber & Chakravorti 1974), which means that the Langmuir model suits for a medium concentration range depending on the performance of adsorbent (Kong *et al.* 2011). In the present study, the last point of the Langmuir model slightly deviated from the linear regression (Fig. 5a) and the K_L was 0.09 for the last point, which was close to 0, indicating that the description of the removal of Cr(VI) by BC400/2 was more accurate at a Cr(VI) concentration below 100 mg/L than at high Cr(VI) concentration when using the Langmuir model.

Freundlich model (Fig. 5b) is more practical for the process of adsorption that doesn't just happen in the surface layer and energy distribution is not even for each adsorption site (Febrianto *et al.* 2009). A value of 3.20 for the characteristic parameter "n" was obtained, signifying that the reaction was preferential (Farooq *et al.* 2010).

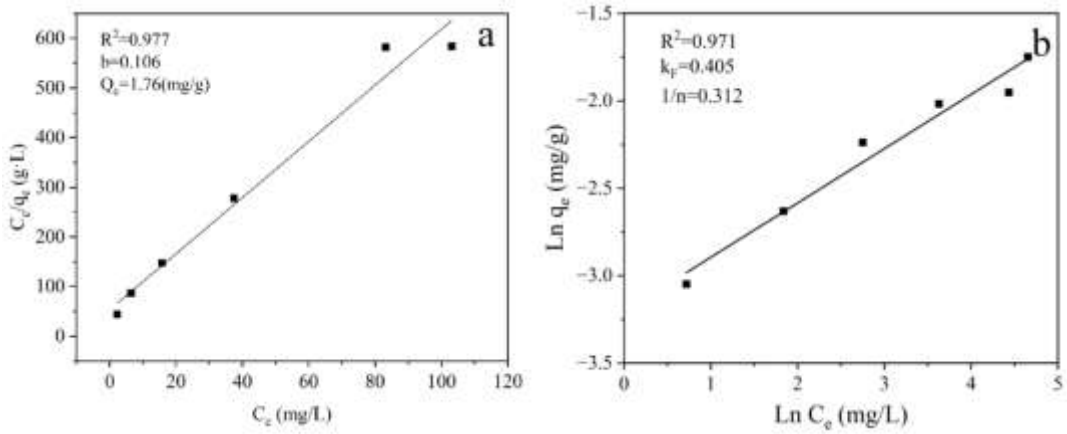

Fig. 5. Langmuir and Freundlich models of Cr(VI) adsorption by BC400/2. (a) Langmuir model; and (b) Freundlich model.

3.4. Cr(VI) Removal Mechanism

3.4.1. Surface morphology of BC400/2

To better understand the reaction between BC400/2 and Cr in solution, the morphology of BC400/2 was scanned. After adsorption, the surface of the sample showed tiny voids (Fig. 6a, b). Spherical morphology similar to that of previous scanning result (Trimukhe & Varma 2008), which suggested that the morphology of BC400/2 after adsorption was similar to that of chitosan (deacylated chitin). Chitin was considered to be one of the major components in the skin of silkworm pupa (McKay *et al.* 1999), which had a lattice-like morphology (Minke & Blackwell 1978). The pyrolysis process remained partially of the spherical structure of chitosan. There was no wide range of porous channels compared to wood pellets derived biochars prepared under 900 ℃ in gasification process (Muvhiiwa *et al.* 2019).

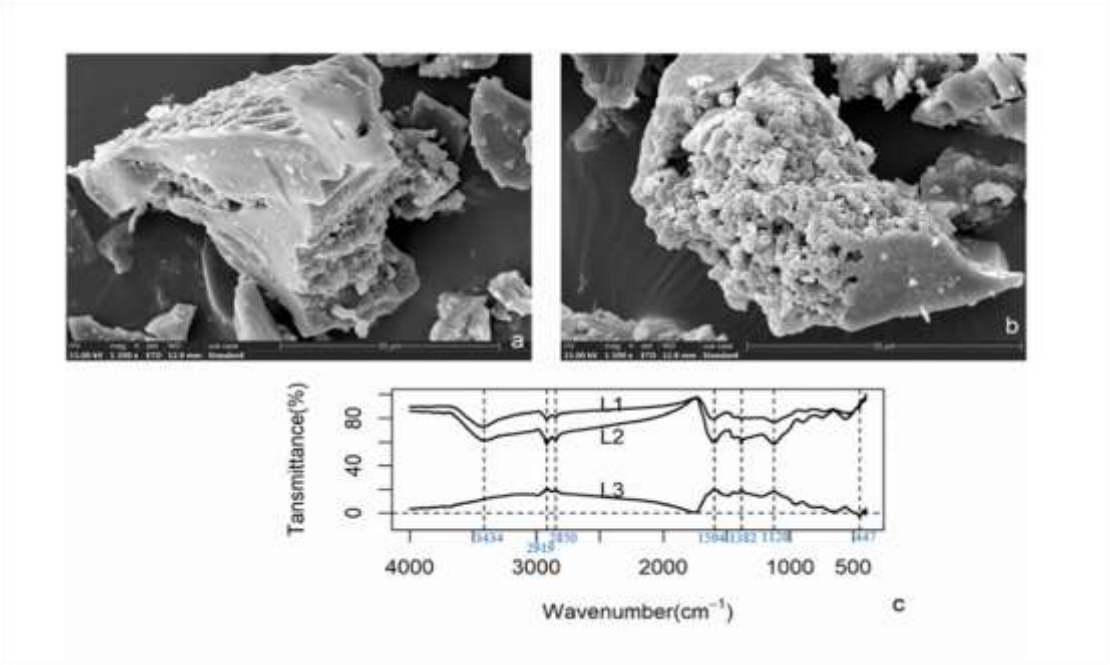

Fig. 6. Scanning electron microscope (SEM) images and FTIR spectras of BC400/2. (a) SEM images before adsorption under the magnification of 1200; (b) SEM images after adsorption under the

magnification of 1500, the white horizontal lines at the right bottom in both figures represent the length of 50 μm; (c) FTIR spectra of BC400/2 before (L_2) and after (L_1) Cr(VI) adsorption as well as transmittance change (L_3), the horizontal line represents no transmittance change after adsorption

3.4.2 Functional Groups of BC400/2

FTIR spectra was used to explore the functional group changes after Cr adsorption on BC400/2 (Fig. 6c). The peak at 1128 cm^{-1} and 1382 cm^{-1} stood for the systemic vibration of -CH_2- and -C-O-C-, respectively (Qu *et al.* 2000). The peak at 1382 cm^{-1} corresponded to the bonding vibration of -CH_3 (Qu *et al.* 2000). The peak at 1594 cm^{-1} was close to 1595 cm^{-1} which was identified to be the superposition between bands corresponding to the stretching vibrations of conjugated -C=C- bonds and carbonyl groups (Hsu *et al.* 2009). The peak at 2850 cm^{-1} stood for the symmetric expansion of the -CH, and the peak at 2919 cm^{-1} stood for the antisymmetric expansion of the -CH. Furthermore, the broad and strong band at 3434 cm^{-1} is assigned to the overlapping of -NH- and -OH stretching vibrations (Shi *et al.* 2018), which indicated that -OH might participated in the complexation of $HCrO_4^-$. FTIR spectra showed that there were some oxygen-containing functional groups and C=C groups on the surface of the silkworm pupal biochar, which were beneficial to the attachment growth of microorganisms (Bolan *et al.* 2023). These groups could also be used as electron donors to reduce Cr(VI) with strong oxidation ability. Therefore, the existence of these characteristic peaks is conducive to the treatment of Cr(VI) by the silkworm biochar (Ding *et al.* 2021).

The results of FTIR spectra analysis showed the abundance of functional groups in BC400/2, including C-O, C=C, O-H and -NH_2 (Fig. 6c). Therefore, the possible reaction mechanism for the removal of Cr(VI) by BC400/2 was proposed [Eqs.(2~4)] (Ma *et al.* 2021).

$$HCrO_4^- + 7H^+ + 3e^- \rightarrow Cr^{3+} + 4H_2O \quad (2)$$

Simultaneously, the amino-functional groups (-NH_2) could be protonated to -NH_3^+ under acidic conditions as well as -OH which also could be protonated to -O.

$$-R - NH_2 + H^+ + HCrO_4^- \rightarrow -R - NH_3 - HCrO_4^- \quad (3)$$

$$-R - OH + HCrO_4^- + 4H^+ \rightarrow -R - O + Cr^{3+} + 4H_2O \quad (4)$$

Based on the experimental results, a mechanism for Cr(VI) removal by BC400/2 is proposed that Cr(VI) diffused from the aqueous phase to the surface and pores of the adsorbent by film diffusion and molecular diffusion, and then Cr(VI) was further adsorbed on BC400/2 by chemical adsorption. The chemisorption was driven by the ionic interaction between Cr(VI) and the functional groups (i.e. C-O, C=C, O-H and -NH_2) of the biochar (Ma *et al.* 2021). The high removal efficiency of Cr(VI) under low pH conditions was due to the high content of H^+ in the solution, which caused protonation on the surface of BC400/2 and made it positively charged. In addition, Cr(VI) was mainly present in the form of $HCrO_4^-$ in the low pH solution. Therefore, Cr(VI) could be adsorbed on BC400/2 by electrostatic attraction (Jia *et al.* 2021). In addition, the presence of -NH_2 in BC400/2 could further immobilise the adsorbed Cr (Luo *et al.* 2022). In summary, the adsorption of Cr(VI) on BC400/2 included electrostatic attraction, redox, and complexation, in which chemisorption was dominant (Jia *et al.* 2021).

3.5. Feasibility of BC400/2 for the Removal of Cr(VI) from Solution

The cost of general materials mainly includes raw

material cost, transportation cost and production cost. Silkworm pupae is the main by-product of silkworm industry, and the raw material cost of SPB can be ignored. The transportation costs here refer to the costs of diesel fuel used to transport raw materials from the place of origin to the destination. According to the 10 t truck consumes 20 L diesel oil per 100 km, and the market price of diesel oil is around 5.8 yuan/L. Guangxi, Sichuan and Jiangsu provinces are the major sericulture producing areas in China. In these areas we can assume that the distance from the production place to the processing plant is 100 km, and the transportation cost is about 14 yuan/t (Qu, 2021). Production costs refer to the costs of processing raw materials into finished products. Mainly for energy consumption, labor consumption and equipment wear and tear. According to the annual output of 1,000 t of silkworm chrysalis biochar, the fixed investment for the operation equipment is 500,000 yuan, assuming the number of staff is 6, and electricity is the sole power source in the industrial production (Qu, 2021). Detailed workshop production cost is listed in Table 3. The total cost of preparing one ton of SPB is about 1,239.3 yuan. Considering that the Cr removal capacity of the SPB is about 1.476 mg/g, and 3.39 kg is needed for the treatment of water with a concentration of 5 mg/L of 1.0 t of Cr(VI), the cost of the material is about 4.2 yuan. In comparison, one ton of commercial iron powder is 1,500 yuan (Qu, 2021), its Cr removal capacity is about 1.250 mg/g, and the treatment of 1.0 t of Cr(VI) concentration of 5 mg/L water needs commercial iron powder 4.0 kg, equivalent to the material cost of about 6.0 yuan. Compared with other materials for treating Cr(VI) wastewater, it has economic advantages, better performance, good feasibility and popularization.

Table 3 Manufacturing cost of silkworm pupa-derived biochar

Project	Cost (yuan/t)
Raw material cost	0
Transportation cost	14.0
Production cost	1,225.3
Electricity bill	474.8
Employee's salary	648.0
Manufacturing cost	102.5
Labor insurance office	*15.0*
Equipment depreciation	*47.5*
Safety and environment protection	*15.0*
Maintenance and transportation	*25.0*
Silkworm pupa-derived biochar cost	1,239.3

4. Conclusions

In this study, the removal of Cr(VI) by silkworm pupae biochar was found to be most effective under strongly acidic conditions (pH < 3), at a mild temperature of 15°C, and with a low adsorbent dosage below 5 g/L. Cr(VI) adsorption by the silkworm pupae biochar is not only monolayer adsorption, but that membrane diffusion and intraparticle diffusion occur simultaneously. At the optimum temperature, the interaction between silkworm pupae biochar and Cr(VI) occurs mainly in the monolayer and most of the Cr(VI) is irreversibly adsorbed. The adsorption of Cr(VI) on BC400/2 included electrostatic attraction, redox and complexation, with chemisorption being dominant. With certain economic advantages, good performance, feasibility and popularity, silkworm-derived biochar is a potential material that can be used to

treat Cr(VI) wastewater. However, the effect of co-existing substances in wastewater on biochar adsorption was not included in this study. Further research is needed to improve the adsorption capacity over a wider pH range for application.

Highlights

- Silkworm pupae, an abundant agricultural residue, were converted into biochar for Cr(VI) removal from water.
- Biochar produced at 300 °C demonstrated effective Cr(VI) adsorption under acidic, low-temperature, and low-dosage conditions.
- The adsorption process involved both membrane and intraparticle diffusion.
- Oxygen-containing and C=C functional groups played key roles in the adsorption mechanism.

Acknowledgement

This study was supported by Science and Technology Innovation Project of Sichuan Provincial Department of Ecology and Environment (ZX-2025019). The authors would like to thank the anonymous reviewers for their helpful comments and suggestions.

Conflict of Interest

The authors declare that there is no conflict of interest.

References

1. Ahmad, M., Rajapaksha, A. U., Lim, J. E., Zhang, M., Bolan, N., Mohan, D., Vithanage, M., Lee, S. S., Ok, Y. S. (2014) Biochar as a sorbent for contaminant management in soil and water: A review. *Chemosphere*, ***99***, 19-33. DOI10.1016/j.chemosphere.2013.10.071
2. Altomare, A. A., Baron, G., Aldini, G., Carini, M., D'Amato, A. (2020) Silkworm pupae as source of high-value edible proteins and of bioactive peptides. *Food Science & Nutrition*, ***8*(6)**, 2652-2661. DOI10.1002/fsn3.1546
3. Altundogan, H. S. (2005) Cr(VI) removal from aqueous solution by iron (III) hydroxide-loaded sugar beet pulp. *Process Biochemistry*, ***40*(3-4)**, 1443-1452. DOI10.1016/j.procbio.2004.06.027
4. Álvarez-Ayuso, E., García-Sánchez, A., Querol, X. (2007) Adsorption of Cr(VI) from synthetic solutions and electroplating wastewaters on amorphous aluminium oxide. *Journal of Hazardous Materials*, ***142*(1-2)**, 191-198. DOI10.1016/j.jhazmat.2006.08.004
5. Aydın, Y. A., Aksoy, N. D. (2009) Adsorption of chromium on chitosan: Optimization, kinetics and thermodynamics. *Chemical Engineering Journal*, ***151*(1-3)**, 188-194. DOI10.1016/j.cej.2009.02.010
6. Beesley, L., Moreno-Jiménez, E., Gomez-Eyles, J. L. (2010) Effects of biochar and greenwaste compost amendments on mobility, bioavailability and toxicity of inorganic and organic contaminants in a multi-element polluted soil. *Environmental Pollution*, ***158*(6)**, 2282-2287. DOI10.1016/j.envpol.2010.02.003
7. Bolan, Shiv., Hou, Deyi., Wang,L.,W., Hale,L., Egamberdieva, D., Tammeorg, P., Li, R., Wang, B., Xu, J., P., Wang, T., Sun, H., W., Padhye, L., P., Wang, H., L., Siddique, K., H.M., Rinklebe, J., Kirkham, M.B., Bolan, N., (2023) The potential of biochar as a microbial carrier for agricultural and environmental applications. Science of the Total Environment ***886***:163968. DOI10.1016/j.scitotenv.2023.163968
8. Braadbaart, F., Poole, I. (2008) Morphological, chemical and physical changes during charcoalification of wood and its relevance to archaeological contexts. *Journal of Archaeological Science*, ***35*(9)**, 2434-2445. DOI10.1016/j.jas.2008.03.016
9. Cantrell, K. B., Hunt, P. G., Uchimiya, M., Novak, J. M., Ro, K. S. (2012) Impact of pyrolysis temperature and manure source on physicochemical characteristics of biochar. *Bioresource Technology*, ***107***, 419-428. DO

I10.1016/j.biortech.2011.11.084
10. Chen, X., Chen, G., Chen, L., Chen, Y., Lehmann, J., McBride, M. B., Hay, A. G. (2011) Adsorption of copper and zinc by biochars produced from pyrolysis of hardwood and corn straw in aqueous solution. *Bioresource Technology*, ***102*****(19)**, 8877-8884. DOI10.1016/j.biortech.2011.06.078
11. Dakiky, M., Khamis, M., Manassra, A., Mer'eb, M. (2002) Selective adsorption of chromium（VI） in industrial wastewater using low-cost abundantly available adsorbents. *Advances in Environmental Research*, **6(4)**, 533-540. DOI10.1016/S1093-0191(01)00079-X
12. Davis, T. A., Volesky, B., Mucci, A. (2003) A review of the biochemistry of heavy metal biosorption by brown algae. *Water Research*, ***37*****(18)**, 4311-4330. DOI10.1016/S0043-1354 (03)00293-8
13. Di Natale, F., Lancia, A., Molino, A., Musmarra, D. (2007) Removal of chromium ions form aqueous solutions by adsorption on activated carbon and char. *Journal of Hazardous Materials*, ***149*****(1)**, 245. DOI10.10 16/j.jhazmat.2006.11.028
14. Ding, S., Yan, S., Xie, L., Sun, Y., Liu, J., Ma, F., Li, C. (2021) Preparation of Cherry Blossom Biomass Charcoal and Adsorption of Hexavalent Chromium in Wastewater. *Applied Chemical Industry*, ***12 vo 50***, 3309-33 14+3319.
15. Dong, X., Ma, L. Q., Li, Y. (2011) Characteristics and mechanisms of hexavalent chromium removal by biochar from sugar beet tailing. *Journal of Hazardous Materials*, ***190*****(1-3)**, 909-915. DOI10.1016/j.jhazmat.20 11.04.008
16. Du, W. L., Xu, Z. R., Han, X. Y., Xu, Y. L., Miao, Z. G. (2008) Preparation, characterization and adsorption properties of chitosan nanoparticles for eosin Y as a model anionic dye. *Journal of Hazardous Materials*, ***153*****(1-2)**,152-156. DOI10.1016/j.jhazmat. 200 7.08.040
17. Farooq, U., Kozinski, J. A., Khan, M. A., Athar, M. (2010) Biosorption of heavy metal ions using wheat based biosorbents – A review of the recent literature. *Bioresource Technology*, ***101*****(14)**, 5043-5053. DOI10. 10 16/j.biortech.2010.02.030
18. Febrianto, J., Kosasih, A. N., Sunarso, J., Ju, Y. H., Indraswati, N., Ismadji, S. (2009) Equilibrium and kinetic studies in adsorption of heavy metals using biosorbent: A summary of recent studies. *Journal of Hazardous Materials*, ***162*****(2-3)**, 616-645. DOI10.1016/ j. jhazmat.2008.06.042
19. Giri, A. K., Patel, R., Mandal, S. (2012) Removal of Cr (VI) from aqueous solution by Eichhornia crassipes root biomass-derived activated carbon. *Chemical Engineering Journal*, ***185-186***, 71-81. DOI10.1016/j.cej. 2012.01.025
20. He, R., Yuan, X., Huang, Z., Wang, H., Jiang, L., Huang, J., Tan, M., Li, H. (2019) Activated biochar with iron-loading and its application in removing Cr (VI) from aqueous solution. *Colloids and Surfaces A: Physicochemical and Engineering Aspects*, ***579***, 123642. DOI10.1016/j.colsurfa.2019.12 3642
21. Hsu, N., Wang, S., Lin, Y., Sheng, G. D., Lee, J. (2009) Reduction of Cr(VI) by Crop-Residue-Derived Black Carbon. *Environmental Science & Technology*, ***43*** **(23)**, 8801-8806. DOI10.1021/es901872x
22. Jia, X., Zhang, Y., He, Z., Chang, F., Zhang, H., Wågberg, T., Hu, G. (2021) Mesopore-rich badam-shell biochar for efficient adsorption of Cr(VI) from aqueous solution. *Journal of Environmental Chemical Engineering*, ***9*****(4)**, 105634. DOI10.1016/j. jece.2021.105634
23. Keiluweit, M., Nico, P. S., Johnson, M. G., Kleber, M. (2010) Dynamic molecular structure of plant biomass-derived black carbon (biochar). *Environmental Science &*

Technology, ***44*****(4)**, 1247-1253. DOI10.1021/es9031419

24. Kołodyńska, D., Wnętrzak, R., Leahy, J. J., Hayes, M. H. B., Kwapiński, W., Hubicki, Z. (2012) Kinetic and adsorptive characterization of biochar in metal ions removal. *Chemical Engineering Journal*, ***197***, 295-305. DOI10.1016/j.cej.2012.05.025
25. Kong, H., He, J., Gao, Y., Wu, H., Zhu, X. (2011) Cosorption of phenanthrene and mercury(II) from aqueous solution by soybean stalk-based biochar. *Journal of Agricultural and Food Chemistry*, ***59*****(22)**, 12116-12123. DOI10.1021/jf202924a
26. Kotaś, J., Stasicka, Z. (2000) Chromium occurrence in the environment and methods of its speciation. *Environmental Pollution*, ***107*****(3)**, 263-283.DOI10.1016/S0269-7491(99)00168-2
27. Luo, L., Cheng, S., Yue, L., You, Z., Cai, J. (2022) N-doped biochar from chitosan gel-like solution: Effect of hydrothermal temperature and superior aqueous Cr (VI) removal performance. *Colloids and Surfaces A: Physicochemical and Engineering Aspects*, ***641***,128426.DOI10.1016/j.colsurfa.2022.128426
28. Luo, X., Du, H., Zhang, X., Yang, Y. (2022) Amine-functionalized magnetic biochars derived from invasive plants Alternanthera philoxeroides for enhanced efficient removal of Cr(VI): Performance, kinetics and mechanism studies. *Environmental Science and Pollution Research*, ***29*****(51)**, 78092-78106. DOI10.1007/s11356-022-20987-4
29. Ma, R., Yan, X., Pu, X., Fu, X., Bai, L., Du, Y., Cheng, M., Qian, J. (2021a) An exploratory study on the aqueous Cr(VI) removal by the sulfate reducing sludge-based biochar. *Separation and Purification Technology*, ***276***, 119314. DOI10.1016/j.seppur.2021.119314
30. Mao, Y., Tao, Y., Zhang, X., Chu, Z., Zhang, X., Huang, H. (2023) Removal of Aqueous Cr(VI) by Tea Stalk Biochar Supported Nanoscale Zero-Valent Iron: Performance and Mechanism. *Water, Air, & Soil Pollution*, ***234*****(3)**,149. DOI10.1007/s11270-023-06164-4
31. Maryuk, O., Gładysz-Płaska, A., Rudaś, M. (2005) Adsorption of chromium(VI) ions on a surfactant-modified clinoptilolite. *Przemysl Chemiczny*, ***84***, 360-363.
32. McKay, G., Ho, Y. S., Ng, J. C. Y. (1999) Biosorption of Copper from Waste Waters: A Review. *Separation and Purification Methods*, ***28*****(1)**,87-125. DOI10.1080/03602549909351645
33. Minke, R., Blackwell, J. (1978) The structure of α-chitin. *Journal of Molecular Biology*, ***120*****(2)**, 167-181. DOI10.1016/0022-2836 (78)90063-3
34. Muvhiiwa, R., Kuvarega, A., Llana, E. M., Muleja, A. (2019) Study of biochar from pyrolysis and gasification of wood pellets in a nitrogen plasma reactor for design of biomass processes. *Journal of Environmental Chemical Engineering*, ***7*****(5)**, 103391. DOI10.1016/j.jece.2019.103391
35. Nguyen, B. T., Lehmann, J., Kinyangi, J., Smernik, R., Riha, S. J., Engelhard, M. H. (2009) Long-term black carbon dynamics in cultivated soil. *Biogeochemistry*, **92**, 163-176. DOI10.1007/s10533-008-9248-x
36. Noroozi, B., Sorial, G. A., Bahrami, H., Arami, M. (2007) Equilibrium and kinetic adsorption study of a cationic dye by a natural adsorbent—Silkworm pupa. *Journal of Hazardous Materials*, ***139*****(1)**, 167-174. DOI10.1016/j.jhazmat.2006.06.021
37. Novak, J. M., Lima, I., Xing, B., Gaskin, J. W., Steiner, C., Das, K. C., Ahmedna, M., Rehrah, D., Watts, D. W., Busscher, W. J., Schomberg, H. (2009) Characterization of Designer Biochar Produced at Different Temperatures and Their Effects on a Loamy Sand. *Annals of Environmental Science*, ***3***, 195-206.
38. Onay, O., Kockar, O. M. (2003) Slow, fast

and flash pyrolysis of rapeseed. *Renewable Energy*, ***28*(15)**, 2417-2433. DOI10.1016/S0960-1481(03)00137-X

39. Ozcan, A., Oncu, E., Ozcan, A. (2006) Adsorption of Acid Blue 193 from aqueous solutions onto DEDMA-sepiolite. *Journal of Hazardous Materials*, ***129*(1-3)**, 244-252. DOI10.1016/j.jhazmat.2005.08.037
40. Qu, M. (2021) Sulfidated copper-iron bimetal PRB material for Cr(VI) removal from groundwater: Preparation and application research. MSc Thesis, University of Chinese Academy of Sciences, China. (in Chinese)
41. Sen Gupta, S., Bhattacharyya, K. G. (2011) Kinetics of adsorption of metal ions on inorganic materials: A review. *Advances in Colloid and Interface Science*, ***162*(1-2)**, 39-58. DOI10.1016/j.cis.2010.12.004
42. Shi, S., Yang, J., Liang, S., Li, M., Gan, Q., Xiao, K., Hu, J. (2018) Enhanced Cr(VI) removal from acidic solutions using biochar modified by Fe_3O_4@SiO_2-NH_2 particles. *Science of The Total Environment*, ***628-629***, 499-508. DOI10.1016/j.scitotenv.2018.02.091
43. Suliman, W., Harsh, J. B., Abu-Lail, N. I., Fortuna, A. M., Dallmeyer, I., Garcia-Perez, M. (2016) Influence of feedstock source and pyrolysis temperature on biochar bulk and surface properties. *Biomass and Bioenergy*, ***84***,37-48. DOI10.1016/j.biombioe.2015.11.010
44. Trimukhe, K., Varma, A. (2008) A morphological study of heavy metal complexes of chitosan and crosslinked chitosans by SEM and WAXRD. *Carbohydrate Polymers*, ***71*(4)**, 698-702. DOI 10.1016/j.carbpol.2007.07.010
45. Uchimiya, M., Wartelle, L. H., Klasson, K. T., Fortier, C. A., Lima, I. M. (2011) Influence of pyrolysis temperature on biochar property and function as a heavy metal sorbent in soil. *Journal of Agricultural and Food Chemistry*, ***59*(6)**, 2501–2510. DOI10.1021/jf104206c
46. Wang, J., Wang, S. (2019) Preparation, modification and environmental application of biochar: A review. *Journal of Cleaner Production*, ***227***, 1002-1022. DOI10. 1016/j.jclepro.2019.04.282
47. Wang, M., Yang, L., Zhang, Z., Wu, X., Zhong, X., Jiang, E. (2018) Research on pH and adsorption properties of N and K cations of biochar based on gray value. *China Environmental Science*, ***38*(11)**, 4141. DOI 10.19674/j.cnki.issn1000-6923.2018.0459.
48. Weber, T. W., Chakravorti, R. K. (1974) Pore and solid diffusion models for fixed-bed adsorbers. *AIChE Journal*, ***20*(2)**, 228-238. DOI10.1002/aic.690200204
49. Wiedner, K., Rumpel, C., Steiner, C., Pozzi, A., Maas, R., Glaser, B. (2013) Chemical evaluation of chars produced by thermochemical conversion (gasification, pyrolysis and hydrothermal carbonization) of agro-industrial biomass on a commercial scale. *Biomass and Bioenergy*, ***59***, 264-278. DOI10.1016/j.biombioe.2013.08.026
50. Wilson, M. H., Hossain, N. M., Shakeelur Raheman A.R., Lee, J. S. (2025) All-day desalination and ZLD-oriented brine production using a grass biomass pellet-derived biochar–carbon fabric evaporator. *Chemical Engineering Journal*, ***519***, 165432. DOI10.1016/j.cej.2025.165432
51. Zhang, Q., Meng, J., Liu, J., Wang, G. (2013) Effects of pyrolysis temperature and duration time on pH, carbon and nitrogen contents of biochars produced from three crop residues. *Chinese Journal of Ecology*, ***32*(9)**, 2347-2353. DOI10.13292/j.1000-4890.2013.0327.